Meteorologische Zeitschrift, Vol. **26**, No. 2, 207–222 (published online November 23, 2016)

A freezing rain storm explored with a C-band polarimetric weather radar using the QVP methodology.

Rudolf Kaltenboeck[1*] and Alexander Ryzhkov[1,2,3]

[1]Cooperative Institute for Mesoscale Meteorological Studies, The University of Oklahoma, Norman, OK, USA
[2]NOAA/OAR National Severe Storms Laboratory, Norman, OK, USA
[3]Advanced Radar Research Center, University of Oklahoma, Norman, OK, USA

(Manuscript received May 13, 2016; in revised form August 29, 2016; accepted September 9, 2016)

Abstract

On 23rd December 2012, a warm frontal atmospheric system caused significant freezing rain at the Vienna International Airport. Analyses of Austrian C-band polarimetric weather radar data reveal cloud microphysical insights in the internal structure of such systems accompanied by the transition from snow toward ice pellets and subsequent freezing rain and warm rain. Polarimetric radar data are exploited using a recently suggested quasi-vertical profiles (QVP) technique. This method allows to analyze the evolution of the melting layer height and other important microphysical signatures as well as the following precipitation development with high temporal and vertical resolution. Because the QVP polarimetric radar data are represented in a height vs time format which is fully compatible with the format the data from vertically pointing remote sensors such as cloud radars or wind profilers are displayed, their combined use is very efficient for understanding and monitoring microphysical processes leading to precipitation formation. This is demonstrated by the joint analysis of the polarimetric and profiler data at the Vienna airport. The QVP methodology is particularly effective for monitoring weather in the terminal areas of airports because of its local coverage and high precision as well as its potential for nowcasting. The methodology is very easy to implement and its use along with traditional techniques for weather radar data analysis using PPIs and reconstructed RHIs looks very promising.

Keywords: aeronautical nowcasting, winter weather, freezing rain, warm front, polarized weather radar data, vertical profiles, cloud microphysic, Austria

1 Introduction

1.1 Winter weather hazards to aviation

Winter weather has significant impact on aviation in terms of flight safety and economic aspects. The approach-departure area is particularly vulnerable with the urgent need for the ground operations such as snow removal and deicing (Isaac et al., 2014). Winter weather-related hazards lower the aviation safety and thus cause possible loss of life or equipment (WMO, 2007). In addition, adverse winter weather can cause flight delays and subsequent reduction in the efficiency of air traffic management (ATM) (Keis, 2015). Largest monthly average delays per flight occur during winter months in Europe, when more than 50 % of the winter air traffic flow management delays are attributed to airport weather (e.g., Eurocontrol, 2012, 2013). The dominant winter weather-related hazards to aviation include in-flight icing, freezing rain (FZRA), heavy snowfall (SN), and low visibility or ceiling (WMO, 2007).

In-flight aircraft icing occurs as a result of accretion of supercooled liquid droplets (especially of drizzle size) on the bodyframe of the aircraft (Serke et al., 2011; Zawadzki et al., 2005). FZRA produces both aircraft icing and accumulation of ice on a runway on a contact with the ground (WMO, 2007; Zerr, 1997). In this case, precipitation typically falls from a warm layer of the atmosphere through a cold layer below and continues either as FZRA or ice pellets (PL) if refreezing in a cold layer occurs (Kumjian et al., 2013; Ryzhkov et al., 2014; Reeves et al., 2014). Heavy SN might occur during intense or stationary frontal events (Kaltenboeck et al., 2010; Picca et al., 2014), with possible orographic enhancement or embedded convection and even lightning (Diendorfer et al., 2006; Mäkelä et al., 2013). Heavy SN causes low ceiling and very poor visibility (Rasmussen et al., 1999) which lead to reduction of the capacity of an airport. Beside flight operation, heavy SN and FZRA will disturb the ground handling and airport operation due to runway contamination and reduced friction, which reduce the possible landing cross wind limits.

At the Vienna International Airport (LOWW), 243 METAR observations (taken every 30 minutes) have been affected by freezing precipitation during past 10 winters (2005/6–2014/15) with highest probability of occurrence during morning hours in the second half of winter period (Austro Control, 2016), which is similar to the Cortinas et al. (2004) results in the US. Nevertheless, strong-impact FZRA is a relatively rare event

*Corresponding author: Rudolf Kaltenboeck, Austro Control, Air Navigation Service – Aeronautical Meteorology, Fuerstenweg 180, A-6026 Innsbruck, Austria, e-mail: rudolf.kaltenboeck@austrocontrol.at

DOI 10.1127/metz/2016/0807

Gebrüder Borntraeger Science Publishers, Stuttgart, www.borntraeger-cramer.com

in Vienna – only 4 % of the previous 243 observations showed moderate intensities. In such cases the anti-icing fluid might not be longer able to prevent the accretion of frozen contaminants on airplanes and even ground handling might be stopped. Reliable nowcasting of the adverse cold-season weather, such as heavy SN, FZRA, or icing would help to warn and prepare pilots, ATM, airport and air operation services for the adequate response.

1.2 Recent work on detection of icing and freezing rain using polarimetric weather radars

Polarimetric weather radar data reveal internal cloud structures and microphysical cloud processes, responsible for precipitation intensification (e.g. Kennedy and Rutledge, 2011), icing hazards (e.g., Williams et al., 2015; Ryzhkov et al., 2011), melting/freezing (e.g., Giangrande et al., 2008), refreezing (Kumjian et al., 2013; Ryzhkov et al., 2011) and changes in precipitation types/visibility (Picca et al., 2014), which are difficult to observe with single-polarization radars.

The radar detection of supercooled liquid water (SLW) which causes in-flight icing of airplanes is difficult. Cloud droplets with typical diameters smaller than 50 µm have very low radar reflectivity and are masked by a few larger ice crystals which dominate the radar return. Additionally, randomly oriented ice crystals and supercooled liquid droplets are both characterized by differential reflectivity (Z_{DR}) and specific differential phase (K_{DP}) close to zero (Ellis et al., 2012). Therefore, vertically pointing radars are utilized to discriminate between SN and supercooled droplets using the difference in their terminal fall speeds (Zawadzki et al., 2005; Fabry et al., 2003). Other instruments like radiometer or lidar are also used (Köhler and Görsdorf, 2014; Isaac et al., 2005). Ikeda et al. (2009) suggested utilizing the reflectivity texture which is smoother for freezing drizzle compared to SN. S-band polarimetric data in the ice-only and mixed-phase clouds were analyzed by Plummer et al. (2010) who observed higher mean values and variances of K_{DP} and Z_{DR} in the ice-only clouds.

The FZRA category is included in some recent versions of the fuzzy-logic hydrometeor classification algorithms which utilize polarimetric radar variables and vertical profiles of temperature retrieved from the output of the numerical weather prediction models (Schuur et al., 2012, 2014; Thompson et al., 2014). An overview of range intervals for different polarimetric radar variables for plates, dendrites, aggregates, sleet or ice pellets and rain (including FZRA) is given in Thompson et al. (2014) for different radar wavelengths and for S band in Griffin et al. (2014). Elevated areas of local maxima of Z_{DR} and K_{DP} accompanied by slight reduction of cross-correlation coefficient (ρ_{hv}) and strong vertical gradient of radar reflectivity (Z) within the temperature interval between −10 and −20 °C were identified by Kennedy and Rutledge (2011), Andrić et al. (2013), and Bechini et al. (2013) as regions of active dendritic particle growth. These regions play important role in the formation of snow precipitation at the surface and the corresponding polarimetric signatures may provide important clues about possible presence of supercooled liquid water there. Williams et al. (2015) claim that the icing hazard is likely absent if differential reflectivity Z_{DR} is anomalously high there (> 5 dB) and the corresponding Z is relatively low which usually happens if the air is saturated with respect to ice but subsaturated with respect to water. Moderate values of Z_{DR} (< 3 dB) and higher values of Z are more indicative of riming and thus are more conducive to icing.

The near-surface refreezing signature (Kumjian et al., 2013; Ryzhkov et al., 2011, 2016) associated with enhanced Z_{DR} marks the transition of FZRA to PL in a subfreezing layer below the elevated temperature inversion. Reeves et al. (2014) point out that clear distinction between PL and FZRA cannot be achieved without information about vertical temperature profiles. Therefore, Ryzhkov et al. (2014) and Reeves et al. (2016) recently suggested using an explicit microphysical model of snow melting/refreezing for discrimination between FZRA and PL.

A novel methodology for processing and presenting polarimetric radar data which has a potential for providing important insight into the intricacies of precipitation formation in mixed-phase clouds was recently introduced by Ryzhkov et al. (2016). It involves azimuthal averaging of Z, Z_{DR}, ρ_{hv}, and differential phase (Φ_{DP}) at high antenna elevation and presenting resulting high-resolution "quasi-vertical profiles (QVPs)" in a height vs time format. The QVP benefits include an ability to examine temporal evolution of microphysical processes governing precipitation production and compare polarimetric data obtained from the scanning surveillance weather radars with observations made by vertically looking remote sensors, such as wind profilers, lidars, radiometers, cloud radars, and radars operating on spaceborne and airborne platforms. These benefits have already been demonstrated for better delineation of the refreezing signature (Ryzhkov et al., 2016) and discrimination between riming (associated with SLW) and aggregation (Kumjian et al., 2016; Giangrande et al., 2016). Riming episodes in these studies were recognized as the reduction of Z_{DR} just above the freezing layer and the "sagging" of the melting layer in terms of polarimetric radar variables.

This study utilizes the QVP methodology to examine C-band polarimetric radar signatures in a winter storm at LOWW accompanied by the transition from SN via PL toward FZRA. The QVP of polarimetric radar variables are complemented and analyzed jointly with simultaneously taken vertical profiles of Doppler velocity measured by a collocated wind profiler.

2 Data and methodology

2.1 Synoptic and surface observation

On 23 December 2012, FZRA occurred at LOWW as a warm front passed over Austria from the west. Warm

air overrode the cold continental air near the surface whereby creating an elevated temperature inversion conducive for a FZRA. In Fig. 1, the frontal precipitation band is shown in the infrared satellite image (ZAMG, 2015) (top panel) and in the Austrian composite of maximum projection of Z (bottom panel). The results of surface observations at LOWW including observed precipitation types are shown in Fig. 2. During the period of SN, PL and FZRA, the surface temperature dropped down below 0 °C. The visibility measured by the Vaisala sensor FD12 reached lowest values close to 1 km (moderate level according to Rasmussen et al., 1999) during SN and increased up to 6 km when the transition to PL and FZRA starts. This period between 08:30 and 09:30 UTC is in the focus of our analysis. Later during the day, significant, long-lasting FZRA occurred and covered all surfaces at the ground and airplanes with clear ice (Fig. 3). This long-lasting adverse weather at the Austrian main airport caused significant problems to airport operations and flight management.

The evolution of the vertical temperature profile during the day is illustrated in Fig. 4 showing how the warm Atlantic air advection from the west aloft was accompanied by a strong northwesterly wind. Cold continental air is advected close to the surface from southeast. At 06:00 UTC, the whole Vienna sounding temperature profile shows negative temperatures which are consistent with snowfall recorded at the surface. FZRA was observed around 12:00 UTC, when the sounding in Fig. 4 shows the development of mid-tropospheric warm air nose with maximum temperature of 3.0 °C favoring FZRA development underneath. Then the minimum temperature in the subfreezing surface layer was −4.1 °C which is above the refreezing threshold (e.g. Reeves et al., 2014) so that raindrops do not refreeze. In the Vienna sounding at 18:00 UTC, the warm nose air area aloft increased significantly. Rain (RA) was observed starting from 17:50 UTC even when a shallow cold layer close to the surface still remained. During the afternoon and evening soundings (at 18:00 and 24:00 UTC), the low-level cold air advection from southeast disappeared.

It should be mentioned that regional and global numerical forecast models such as Consortium for Small-scale Modeling (COSMO-EU) – see COSMO consortium (2016) or Schulz and Schättler (2014) or European Centre for Medium-Range Weather Forecasts (ECMWF) see ECMWF (2015) were not able to reproduce the complex 2–6 °K temperature inversion within a lowest 2-km atmospheric layer indicated by 6-hour radio soundings in Vienna (comparison not shown).

2.2 Weather radar data

Austrian operational weather radar network consists of 5 EEC C-band dual-polarization weather radars and is operated by aeronautical meteorological service of Austro Control, the Austrian civil air service provider. Details about the radar locations, type, and scanning strategy are given in Kaltenboeck (2012a, b). The interleave antenna scanning prescribes two different half-scans, each consisting of 8 elevation tilts which requires scan time of 2.5 min, followed every 15 min by the vertical Z_{DR} bird-bath calibration scan. Locations of the two weather radars used in this study are indicated in Fig. 1. Both radars are situated on the foothills north and east of the Alps in the low land. Weather radar Rauchenwarth (WXR RAU) is located about 5 km west of LOWW, and the Feldkirchen radar (WXR FEL) is about 31 km northeast of the Salzburg airport (LOWS). The radars operate in the simultaneous transmission/reception mode and measure Z_{DR}, ρ_{hv}, and Φ_{DP} in addition to Z. K_{DP} is derived by applying moving average of Φ_{DP} with a small window size of 1.25 km (+/−2 range bins) to resolve winter signatures of K_{DP}. In comparison with summer cases when the resonance backscattering effects at C band are common in heavy rain and hail, (e.g., Kaltenboeck and Ryzhkov, 2013), the contribution of the backscatter differential phase to Φ_{DP} is much smaller in winter and can be neglected as well as attenuation-related biases of Z and Z_{DR}.

Austrian radar radomes are not heated and accumulation of snow on their surfaces can produce significant azimuthally-modulated biases in Z_{DR} depending on the thickness of snow layer as a function of wind direction (e.g., Hudak et al., 2006; Kaltenboeck et al., 2015).

Concurrently collected data from the 1.28 GHz-Radian LAP300 wind profiler – at LOWW are investigated to estimate terminal fall velocities of hydrometeors with high spatial and temporal resolution. The vertical resolution is 45/210 m in low/high modes; update time is 15 min for Doppler moments and 3 min for spectral data. Robust performance of this particular profiler in measuring terminal velocities of hydrometeors and for detection of the freezing level has been demonstrated by Baumann-Stanzer (2003). In stratiform precipitation, the vertical air motion is expected to be weak (e.g., Teshiba et al., 2009) and the measured Doppler velocity is mostly determined by the terminal fall speed.

2.3 Quasi-vertical profiles (QVP)

In this study, we use the QVP methodology to represent polarimetric radar data in a height vs time format as prescribed by Ryzhkov et al. (2016). This method helps to reveal a temporal evolution of the vertical structure of clouds and precipitation in terms of polarimetric radar variables with high vertical resolution and statistical accuracy because azimuthal averaging reduces the statistical errors of noisy polarimetric radar estimates if the medium is relatively homogeneous in the horizontal direction as in case of stratiform precipitation. Ryzhkov et al. (2016) pointed out the additional value of QVP for monitoring the quality of polarimetric measurands and, as example, exposing their changes attributed to accumulation of ice and snow on the radome.

In our QVP estimation, we only retain the gates where $Z \geq 10\,dBZ$ and $\rho_{hv} \geq 0.6$ in order to mitigate possible contamination from nonmeteorological echo.

a)

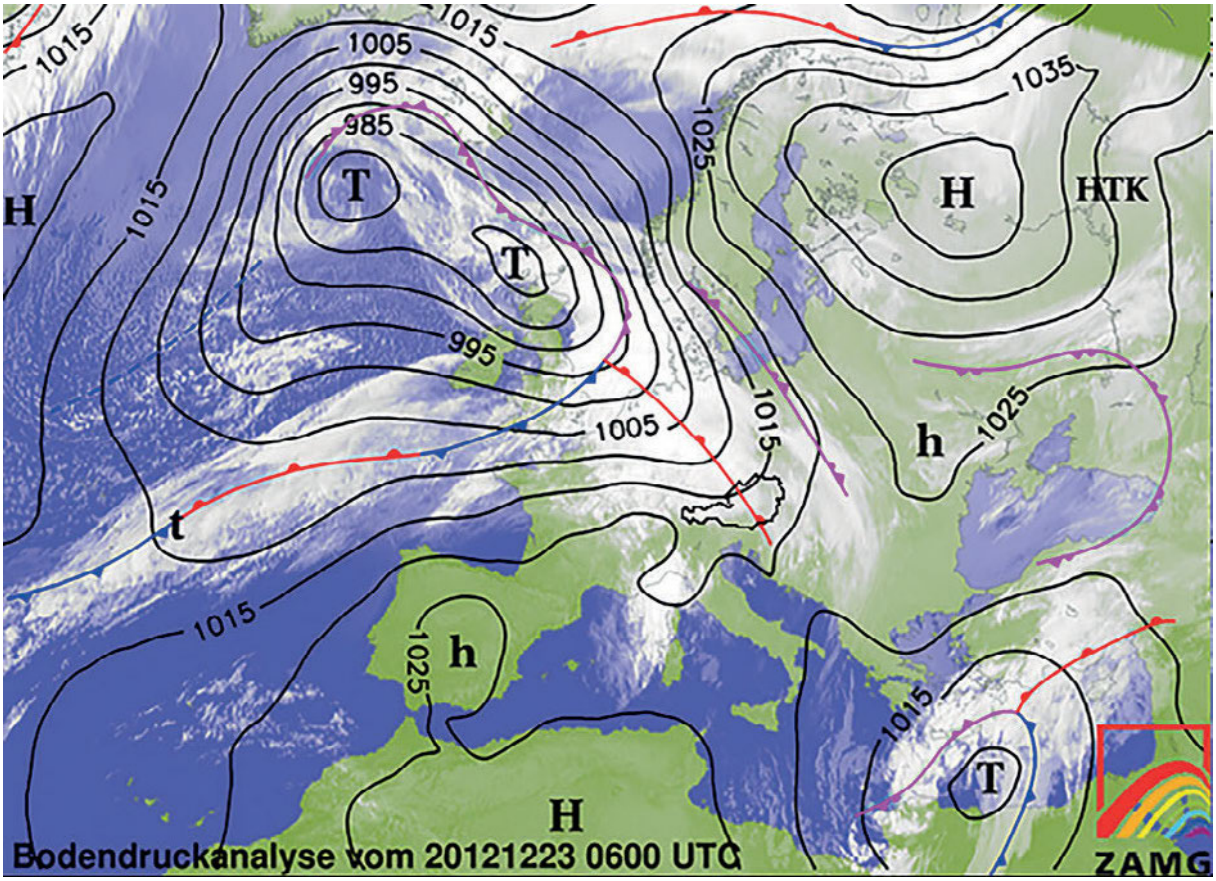

b)

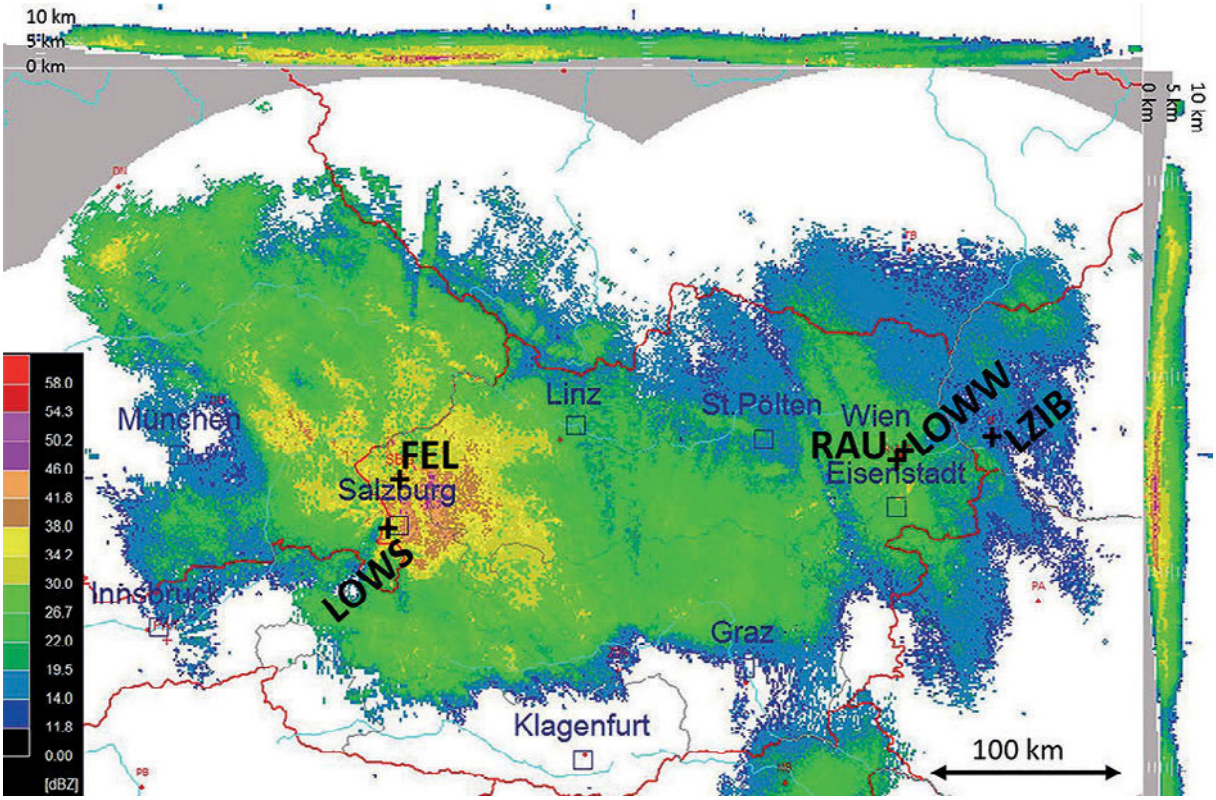

Figure 1: a) European Meteosat infrared (10.8 µm) satellite image with surface pressure isobars and frontal symbols (ZAMG, 2015) overlaid for 23rd Dec. 2012 06:00 UTC. T/H indicates low/high pressure center. b) Austrian composite of maximum projected reflectivity shows the warm frontal rain band over the Alps at 06:00 UTC. Red lines denote country borders. "+" signs denote weather radar Rauchenwarth (RAU) close to Vienna International Airport (LOWW), Bratislava (LZIB) and weather radar Feldkirchen (FEL) northeast of Salzburg International Airport (LOWS).

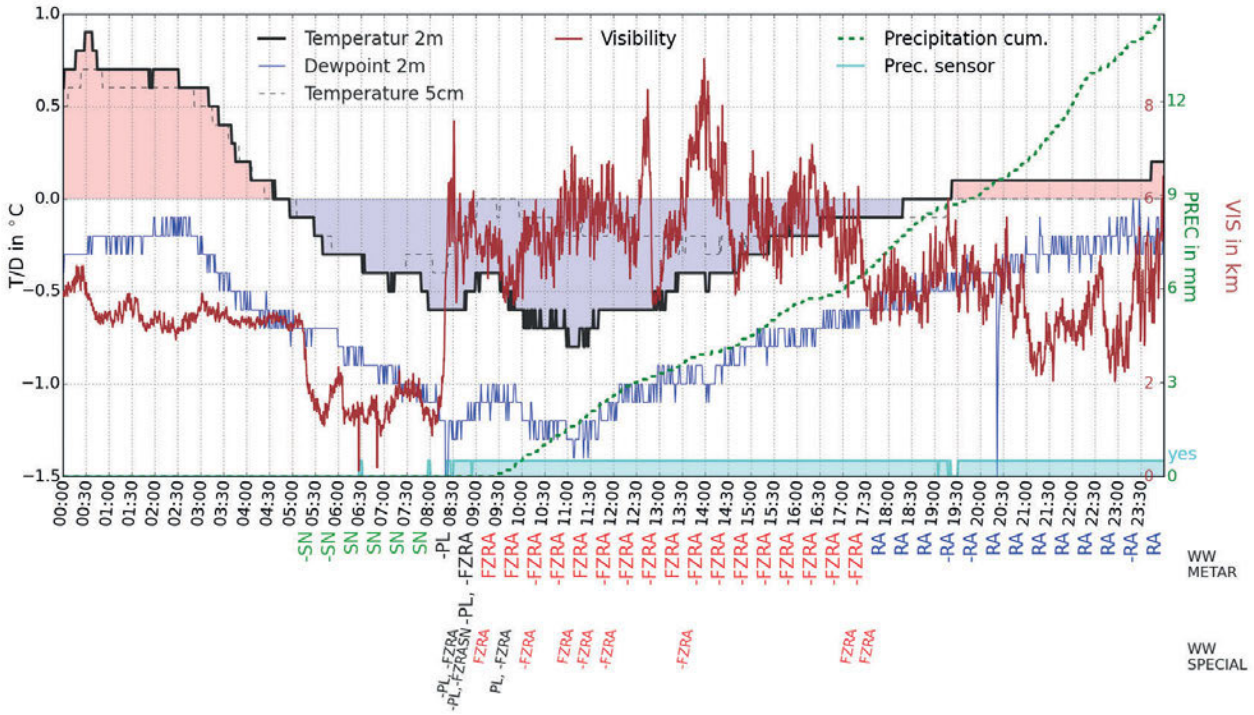

Figure 2: 24-hour surface observations of temperature, dewpoint (−1.5 to 1 °C), precipitation total (0–15 mm), and visibility (0–10 km) at the Vienna International Airport (LOWW) on 23rd December 2012. Human observations of weather (precipitation type) are indicated as METAR abbreviation in different colors: green/snow/SN, black/ice pellets/PL, red/freezing rain/FZRA and blue/rain/RA. METAR observation are reported every 30 minutes (hh:20; hh:50), while SPECIAL are reported when weather significant changes occur.

a) b)

Figure 3: a) Photo of freezing rain and icicle on aircraft wings at the Vienna airport (courtesy by O. Reuss, VIE): b) The photo of ice accumulated during freezing rain taken at the top of the tower of the Vienna airport (courtesy by K. Unger, Austro Control) after the event on 25th December 2012.

For both radars, WXR RAU and WXR FEL, the antenna elevations between 15 and 18° were mainly used to generate QVPs. Therefore, the corresponding diameter of the averaging area at a 5 km height varies between 28 and 34 km.

The sensitivity of QVP to elevation angle and the radome influence is discussed in the following Section 3.3.

3 Results and discussion

3.1 General radar features of the storm system

Figs. 5 and 6 show the QVPs of Z, Z_{DR}, ρ_{hv}, and Φ_{DP} for the whole period of warm frontal passage over WXR RAU and WXR FEL respectively. Three major obvious

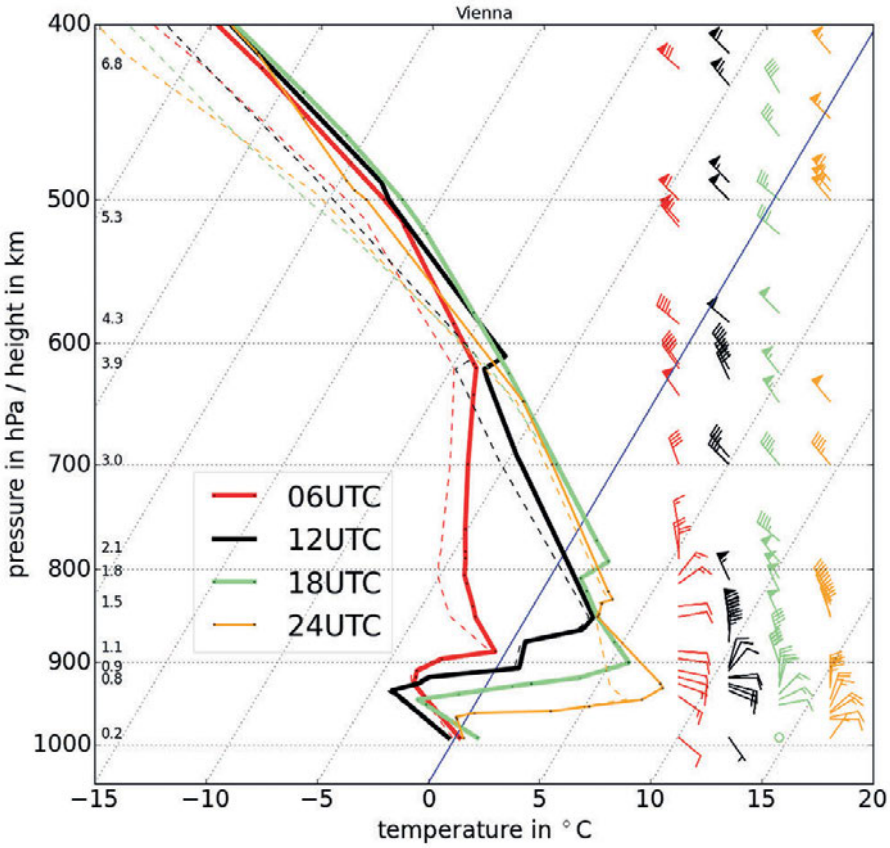

Figure 4: Skew T-log p diagram of the 6 hourly soundings from Vienna on 23rd December 2012 showing the warm air advection above the cold surface layer during the day. Solid and dashed lines represent temperature and dewpoint respectively. A 0 °C isotherm is drawn in solid blue. Wind barbs are given in knots (half/full barbs are 5/10 kt, and flags are 50 kt). Note that snow fell around 06:00 UTC (red solid line), freezing rain was observed around 12:00 UTC (black), and rain started around 18:00 UTC (green).

features in the QVPs for both radars are associated with (a) the melting layer, (b) the dendritic growth layer, (c) and the riming regions.

a) Melting layer (ML). The ML is characterized by enhanced values of Z (up to 30 dBZ) and Z_{DR} (up to 3 dB) and decreased ρ_{hv} (down to 0.9) typical for S and C bands (e.g., Giangrande et al., 2008; Kaltenboeck, 2012a). The ML is also manifested by a bump in the vertical profiles of Φ_{DP} attributed to the backscatter differential phase (Troemel et al., 2014; Ryzhkov et al., 2016). The ML first set off in the Salzburg area at about 22:00 UTC on 22 December (Fig. 6) and showed up near the Vienna airport 10 hours later at 08:00 UTC the next day following eastward progression of warm air. Later on, the ML designated by the radars reached the height of about 2 km above sea level in both locations in good agreement with the model-based 0° isotherm (marked by a dotted line) which is situated slightly higher, as expected. At the Vienna location, the radar designation of the ML onset is apparently more accurate than obtained from the model analysis which shows first appearance of a "warm nose" aloft almost 2 hours later (Fig. 5).

b) Dendritic growth layer (DGL). Another notable radar signature is associated with the DGL within a height interval between −10 and −20 °C. It is characterized by strong vertical gradient of Z, the increase of Z_{DR}, and reduction in ρhv. The maximal values of Z_{DR} are reached close to the height of the −15 °C isotherm marked by a dotted line. Below the DGL, Z_{DR} decreases due to aggregation and/or riming because aggregation reduces bulk density of snowflakes and riming makes them more spherical. There are interesting differences between vertical profiles of radar variables in Fig. 5 and 6. The storm system was apparently shallower during its passage over Vienna. As a result, it is likely that the concentration of initially nucleated ice at the top of the storm is lower for the Vienna episode. This may explain why aggregation is obviously stronger during the Salzburg phase as revealed by steeper decline of Z_{DR} below the DGL and stronger vertical gradient of Φ_{DP} or K_{DP} which is proportional to a total concentration of ice particles. The magnitude of Z_{DR} is lower in the DGL over Salzburg. This can be explained by the fact that the Z_{DR} signature is masked by abundance of more isometric crystals falling from higher altitude and a larger number of crystals compete with each other for available water vapor so that none of them grows too large to produce really high Z_{DR}. Although we observe this interesting phenomenon repeatedly in a number of QVPs in various storms, our interpretation of it is speculative at the moment and requires substantiation via analysis of in situ aircraft data.

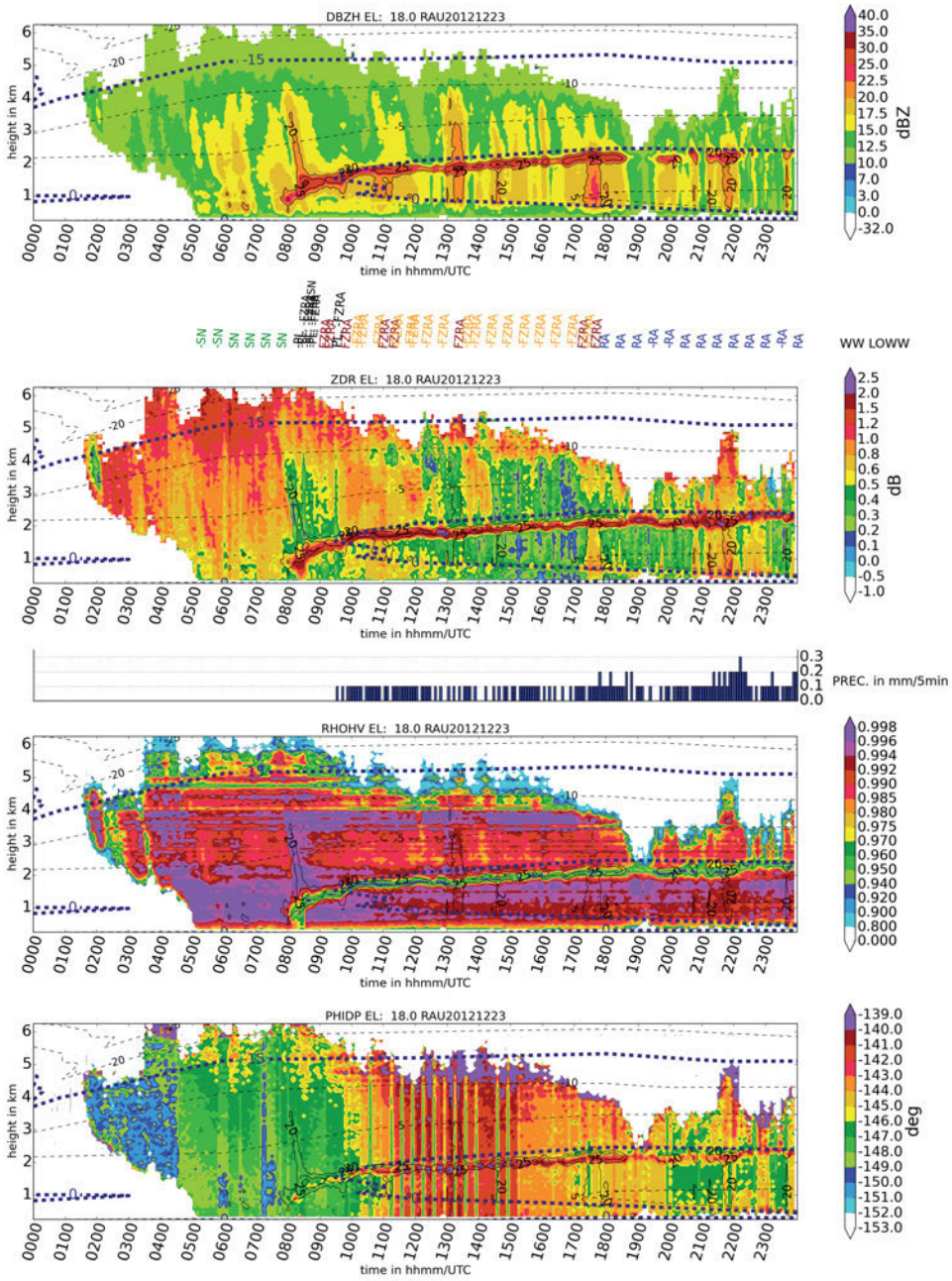

Figure 5: The height vs time representation of quasi-vertical profiles (QVP) of reflectivity (Z), differential reflectivity (Z_{DR}), cross-correlation coefficient (ρ_{hv}) and differential phase (Φ_{DP}) (starting from top) retrieved from the radar data, collected at elevation 18° by the Rauchenwarth (RAU) radar during 24 hours of the Vienna Christmas winter storm on 23rd December 2012 (scans are updated every 5 minutes). Overlaid are contours of temperature retrieved from 6 hourly radio soundings in Vienna as dashed lines (−15/0 °C in dark blue) and 20/25/30 dBZ radar reflectivity as solid line. Transition from snow (green, 05:00–08:30 UTC) to ice pellets (black, 08:30–09:30 UTC) toward freezing rain (orange, 09:30–18:00 UTC) and rain (blue, after 18:00 UTC) is indicated by METAR abbreviations between the plots. Precipitation intensity (mm in 5 min) is given as bar plot below the QVP Z_{DR} panel. Height is given in km above sea level.

c) Riming. Figs. 5 and 6 exhibit several episodes of riming. As shown in Ryzhkov et al. (2016) and Kumjian et al. (2016), riming can be identified in the QVPs by enhanced Z, depressed Z_{DR} just above the freezing level, and by the "sagging" of the melting layer. The enhancement in Z is attributed to a more intense growth of ice particles via deposition of vapor and accretion of supercooled cloud droplets in the convective updrafts. Riming makes snowflakes more spherical and, as a result, Z_{DR} of rimed snowflakes is usually lower than the one of unrimed aggregated snow (see also Vogel et al., 2015). Due to their higher density, rimed snowflakes fall faster within the melting layer and their complete melting occurs at lower heights which explains the "sagging" of the ML in terms of Z_{DR} and ρ_{hv}. Obvious signatures of riming are visible in the Vienna QVPs

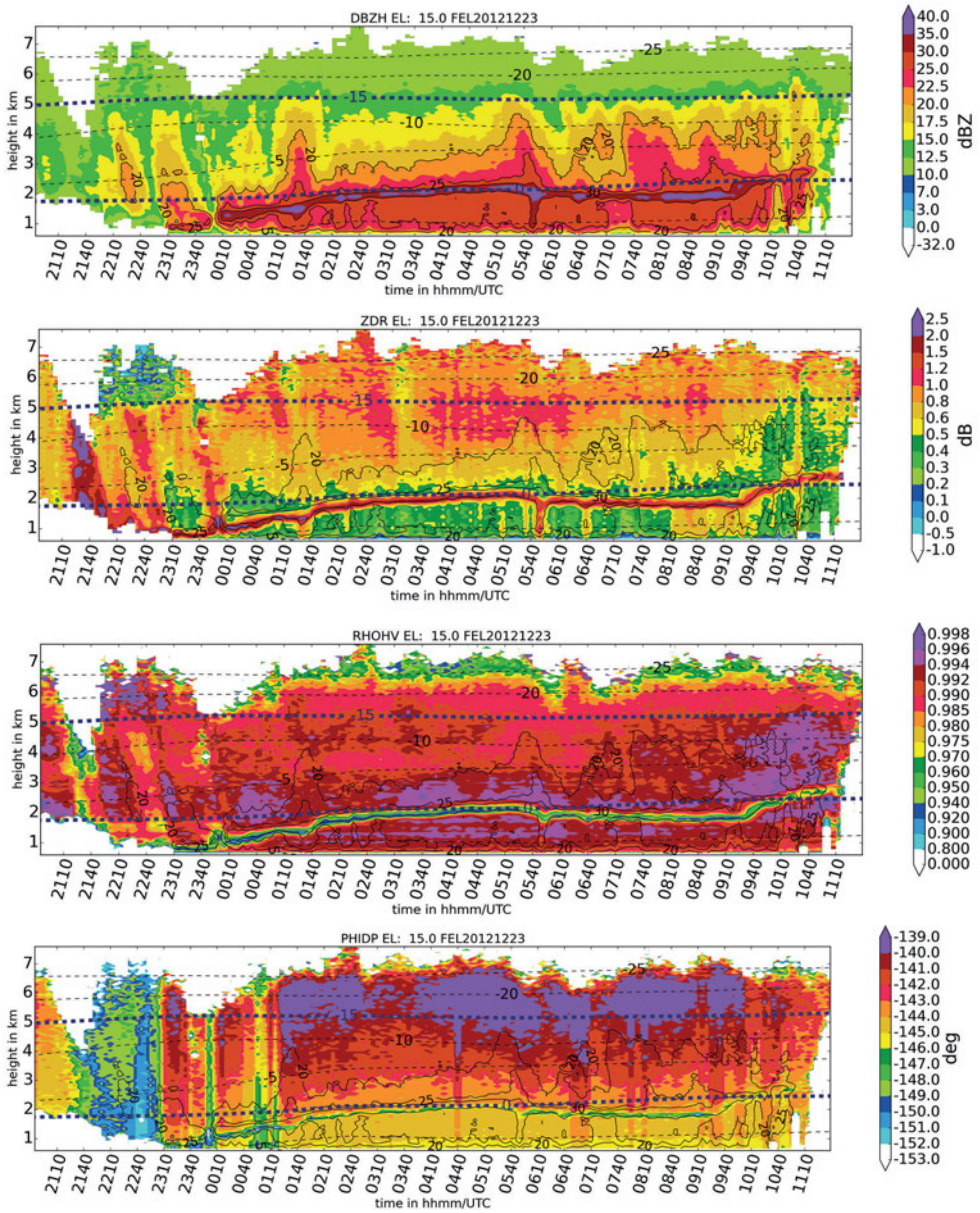

Figure 6: as Fig. 5 but for weather radar Feldkirchen (FEL, 594 m height) northeast of Salzburg when pure rain was observed at the Salzburg international airport (430 m height). Note a 15-hour time period on the x axis, starting on 22nd December 2012, at 20:40 UTC, and the y axis up to 7.6 km. Temperature (°C) contours are given in dashed black lines for COSMO-EU numerical model forecast at the Salzburg airport (dark blue for 0/−15 °C). The 20/25/30 dBZ radar reflectivity contours are shown by solid lines.

at about 08:30 UTC and 13:00 UTC and in the Salzburg QVPs at 01:40 UTC and 05:40 UTC.

3.2 Temporal evolution of precipitation type at the Vienna airport as revealed from the polarimetric radar and wind profiler data

The north-east progression of the warm front is captured in the series of three PPI images of Z, Z_{DR}, and ρ_{hv} at elevation 1.8° taken at 07:35, 08:35, and 09:35 UTC and displayed in Fig. 7. A mesoscale frontal line (MFL) marked by a dashed curve is accompanied by the increase in Z_{DR} (up to 2–3 dB) and the decrease of ρ_{hv} (down to 0.9). The areas of snow, ice pellets, and freezing rain at the surface are indicated by symbols SN, PL, and FZRA. A sloping melting layer is clearly seen in the RHI images in the bottom panels of Fig. 7 (enclosed in the dashed ovals).

Wave patterns are evident in all PPI plots at 08:35 and 09:35 UTC indicated by symbol W. The waves are generated below 1 km in the layer of strong wind shear and are particularly pronounced when embedded in the melting layer. They might be a possible source for generating local upward and downward motions resulting in the production of supercooled water with associated riming of ice particles (e.g., Grazioli et al., 2015). These waves may also cause temporal oscillations of the height of the melting layer observed in the QVP plots in addition to the "sagging" of the melting layer due to riming.

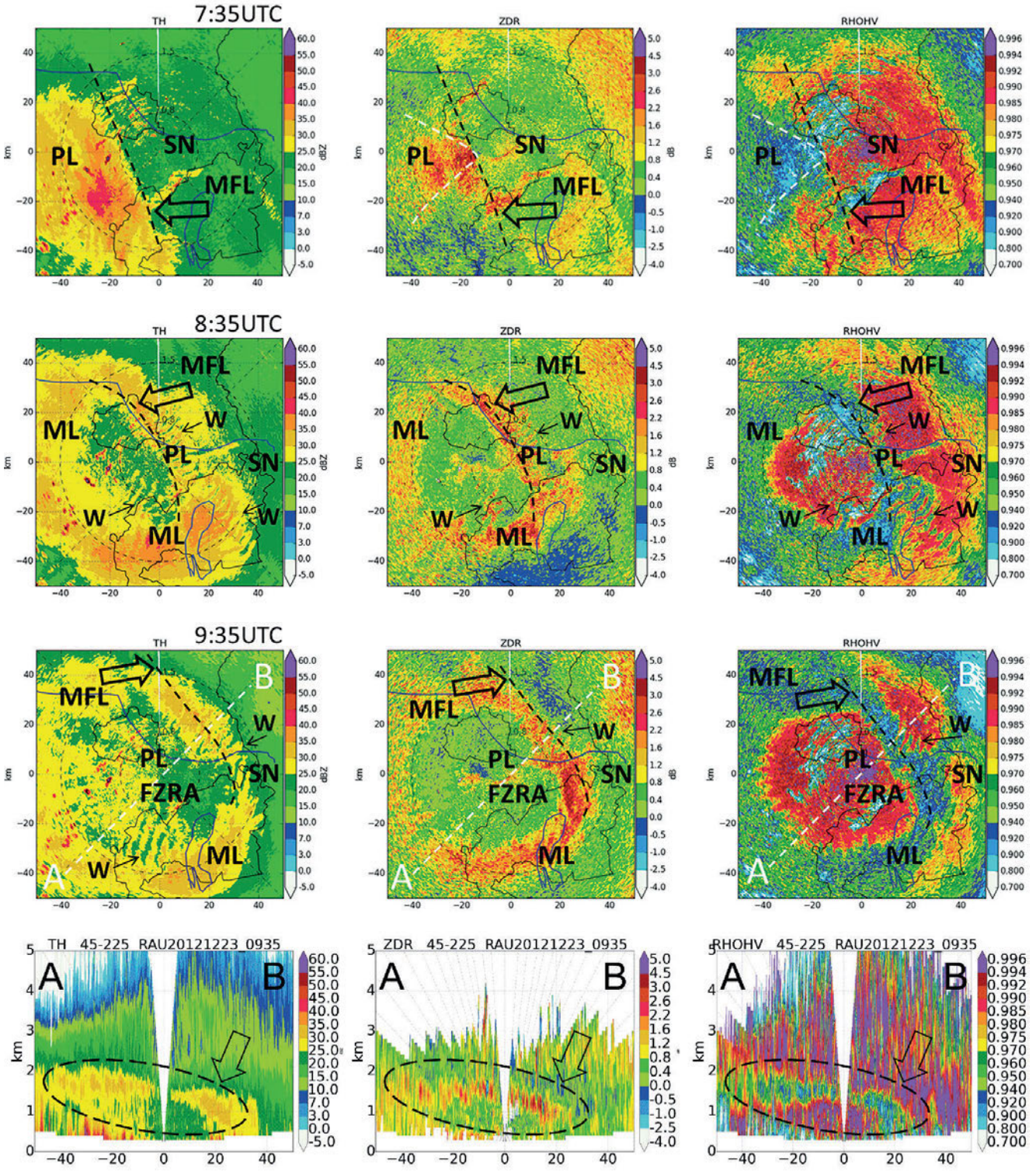

Figure 7: Mesoscale frontal boundaries are shown in composite of PPI and reconstructed RHI (bottom row) of Z (left), Z_{DR} (middle) and ρ_{hv} (right) from WXR RAU elevation 1.8° on 23rd December 2012, at 07:35 (snow at the Vienna airport), 08:35 (ice pellets) and 09:35 UTC (freezing rain) respectively. Position of the RHI (225/45° azimuth; 09:35 UTC) is overlaid as dashed white line (A-B) in PPI images. Labeled dashed circles indicate height msl in km. Location of radar in each panel is at 0, 0 in meridional and zonal axis and the range is given in km (+/−50 km). Arrows label the dashed line of the mesoscale frontal line (MFL) and wave pattern (W). ML marks the melting layer signature. SN, PL and FZRA indicate surface observations of snow, ice pellets, and freezing rain respectively. The vertical cross-section of the melting layer (ML) is shown in a composite RHI (bottom panel) and the ML is enclosed in dashed ellipses. The MFL descending to the surface around 20 km to the east of the radar discriminates between SN to the east and PL and FZRA to the west.

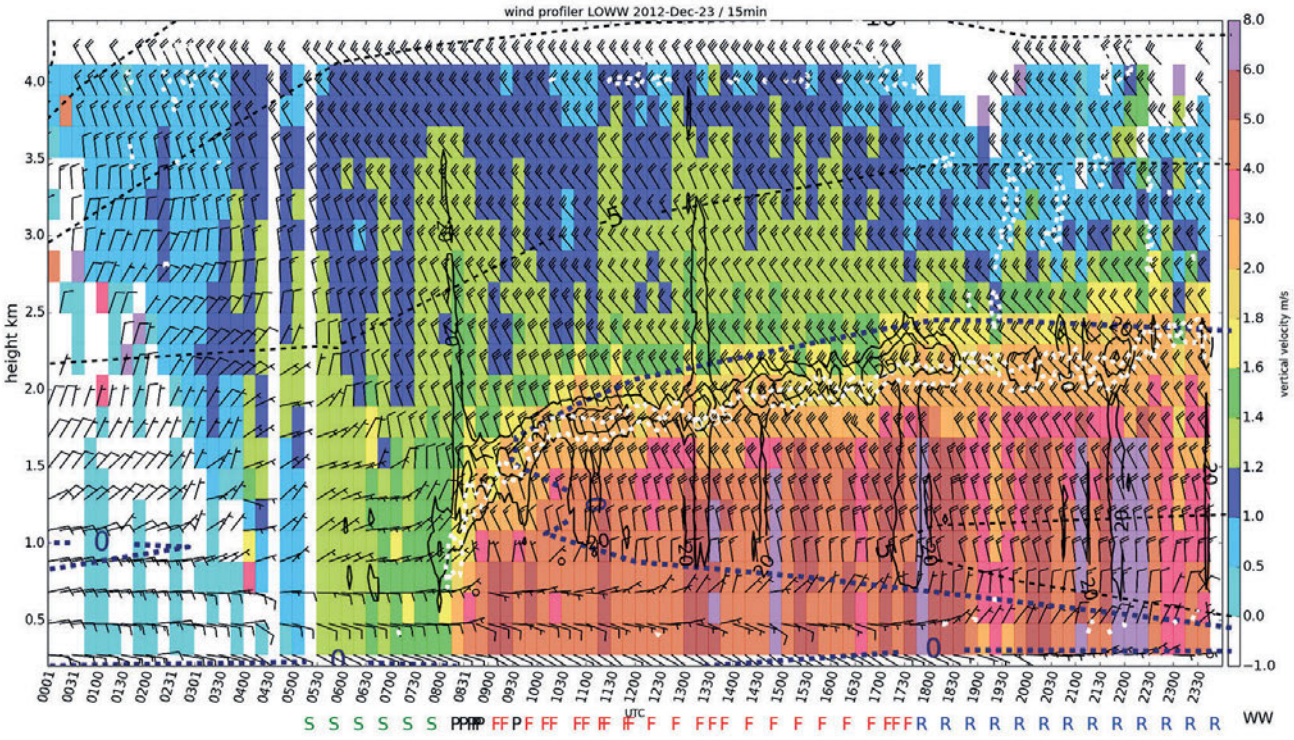

Figure 8: A 24-hour time vs height (km msl) plot of long pulse wind profiler data for 23rd December 2012 in LOWW. The time interval of measurements was 15 minutes. Wind barbs represent horizontal wind in knots. Color-filled contours show vertical velocity obtained from zenith pointing antenna beam (positive when downward; note non-uniform colormap for resolving vertical fall speed of riming periods). Bright band is indicated as black thick contour line, which represents Z 20 and 25 dBZ as well as white dotted ρ_{hv} = 0.95 contour from Fig. 5. As in Fig. 5, isotherms are overlaid in 5 K intervals from sounding Vienna (6 hour intervals) as dashed black/blue lines (blue represents freezing level). Precipitation type from METAR and SPECIAL is indicated below the x-axis (S=SN, P=PL, F=FZRA, R=RA).

The polarimetric radar data are complemented with the data collected by the wind profiler located at LOWW. The profiler data are presented in a height vs time format which is fully compatible with the way QVPs are represented. In Fig. 8, a temporal evolution of horizontal wind and vertical Doppler velocity is displayed with 15-min resolution. Vertical Doppler velocities are color-coded. As in Fig. 5, dotted line depicts the boundary between mid-tropospheric northwesterly flow (warm air advection aloft) and low-level southeasterly wind (surface cold air advection). It should be noted that an outgoing aircraft reported severe turbulence below 760 m at 12:25 UTC along this low level-shear while moderate turbulence was reported at 16:55 UTC for the same heights by an incoming airplane. ATM received no icing reports from pilots during the day. In addition to their mean values, the profiler measured spectra of vertical Doppler velocities at different height levels (Fig. 9).

During the period from 08:00 till 08:20 UTC, the melting layer signature is observed at the surface which is consistent with the transition from dry SN to wet SN and PL reported at LOWW (Fig. 2). This transition was accompanied by abrupt improvement in the visibility at the airport from 1 km to 6 km (Fig. 2). Mean vertical Doppler velocities measured by the profiler are below 1.5 m/s at 08:00 UTC but change dramatically 30–40 min later (Figs. 8 and 9). After 08:30 UTC, the ML ascended rapidly to the heights exceeding 1 km. PL as a primary type of precipitation at the surface were reported from 08:30 to 09:00 UTC. During this period, interesting features are exhibited in the spectra of vertical Doppler velocities measured by the profiler (Fig. 9b). Since we do not expect strong vertical air motions in the surface layer for this type of storm during this time, significant changes of Doppler spectra with height can be attributed to the differences in the terminal velocities of hydrometeors at different altitudes. We speculate that these might be produced either by refreezing of partially melted snowflakes or by advection of hydrometeors of various habits into a vertical column of air probed by the profiler. Refreezing is possible because the air near the surface remained at negative temperatures (Fig. 2) and snowflakes falling through the ML may not melt entirely in the "warm nose" aloft and the resulting raindrops with remnants of ice inside them start refreezing immediately once they enter subfreezing layer next to the surface. During refreezing, a terminal velocity of the hydrometeor may decrease by a factor of 2 as shown in Fig. 10. This explains why radar scatterers have higher terminal velocities aloft before refreezing starts as Fig. 9b shows. An alternative explanation involves advection whereby hydrometeors of different habits and different trajectories show up simultaneously within a vertical column. It is likely that PL formed earlier than raindrops appear closer to the surface than raindrops which just formed below the ML and didn't have enough time to sediment

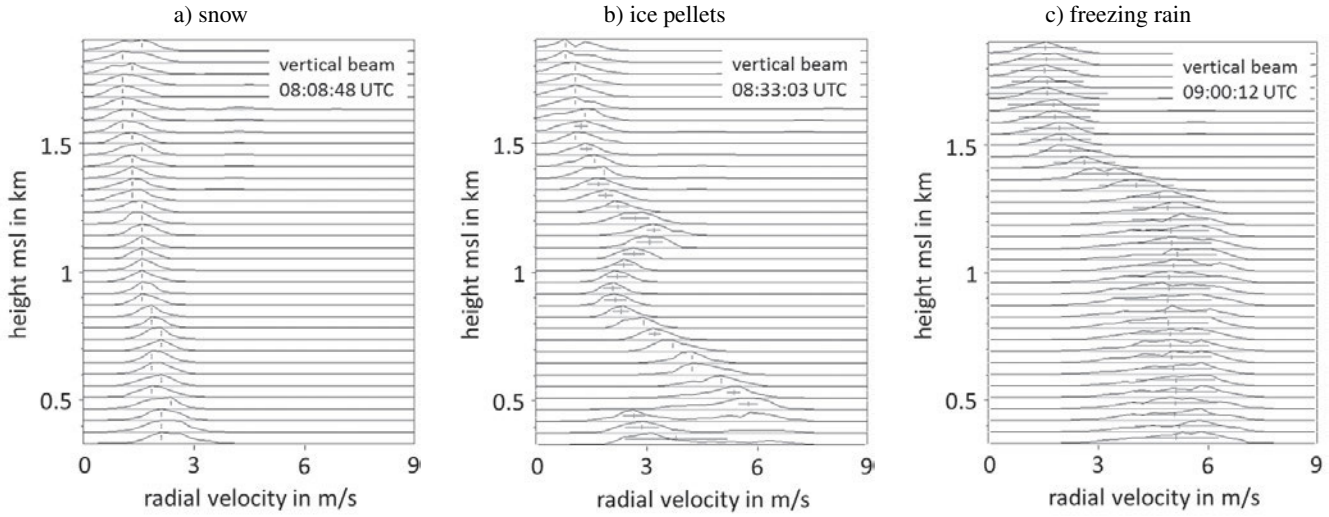

Figure 9: Low mode Doppler spectra measured at the vertical incidence by the wind profiler during the periods of moderate intensities of snow, ice pellets (refreezing) and freezing rain at the Vienna airport. Images from left to right correspond to 08:08, 08:33, and 09:00 UTC on 23rd December 2012 respectively. The 35 curves shows the distribution of vertical velocity (downward when positive – x axis from 0 to 9 m/s) as a function of height (y axis 0.35 to 1.9 km height msl).

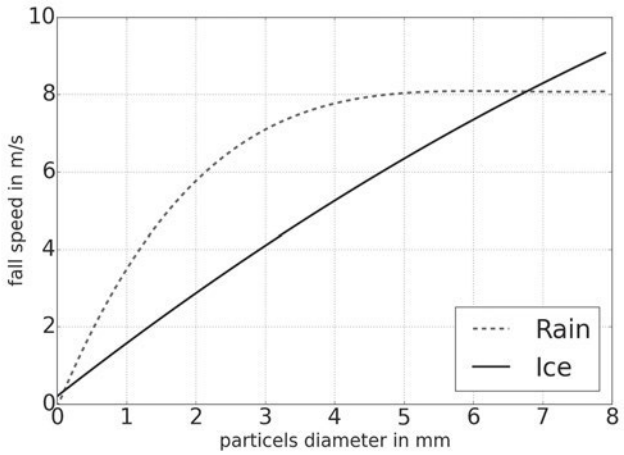

Figure 10: Parameterized particle fall speed as a function of diameter for rain (blue dashed curve) and ice pellets (black solid curve) as used in Kumjian et al. (2012), adapted from Kumjian et al. (2013). p = 942 hPa, T = 284 K

to the lower height levels. The vertical Doppler velocity spectra at later time, 09:00 UTC (Fig. 9c), show uniformly high terminal velocities below 1.3 km which is consistent with purely liquid raindrops or freezing rain because air temperature near the surface still remained negative but the transition process involving hydrometeors of different phase composition was already over.

FZRA at the airport continues for the next 9 hours until 18:00 UTC when the surface eventually warmed up above 0 °C. This type of precipitation is confirmed by the polarimetric radar and wind profiler measurements. The QVP representation of the radar data in a height vs time format in Fig. 5 allows revealing a general correlation between lower values of Z_{DR} within 1–2 km above the freezing level (or the top of the melting layer) and similarly reduced Z_{DR} in rain below the melting level. Such correlation is particularly obvious between 08:00 and 09:30 UTC and between 13:00 and 13:30 UTC. During both time intervals, radar reflectivity in SN aloft is higher than 20 dBZ which may point either to riming or aggregation. Lower Z_{DR} in rain apparently means smaller median diameter of raindrops. We may not exclude that riming aloft results in denser and smaller size snowflakes as opposed to aggregation. After melting, smaller rimed snowflakes produce smaller raindrops. This is generally consistent with experimental evidence that raindrops associated with weak embedded convection are usually smaller than the ones produced in pure stratiform clouds. This is of course not the case for deep convection when large graupel/hail aloft usually melts into very large raindrops.

3.3 QVP sensitivity to the choice of antenna elevation angle

The use of the QVP methodology assumes that the medium is relatively homogeneous in the horizontal direction. In our case, we are dealing with a mesoscale frontal boundary which by definition is a significant horizontal heterogeneity. The question is "how applicable is the QVP technique for monitoring typical frontal conditions often accompanied by dramatic changes of precipitation types at the surface?". The effective horizontal resolution of QVP depends on the height above ground and improves with increasing elevation at which radar data are taken to produce quasi-vertical profiles. In order to explore the impact of the QVP elevation on the interpretation of the radar data, we generated QVPs using the WXR RAU data collected at three antenna elevations: 5.6°, 18°, and 65° (Fig. 11).

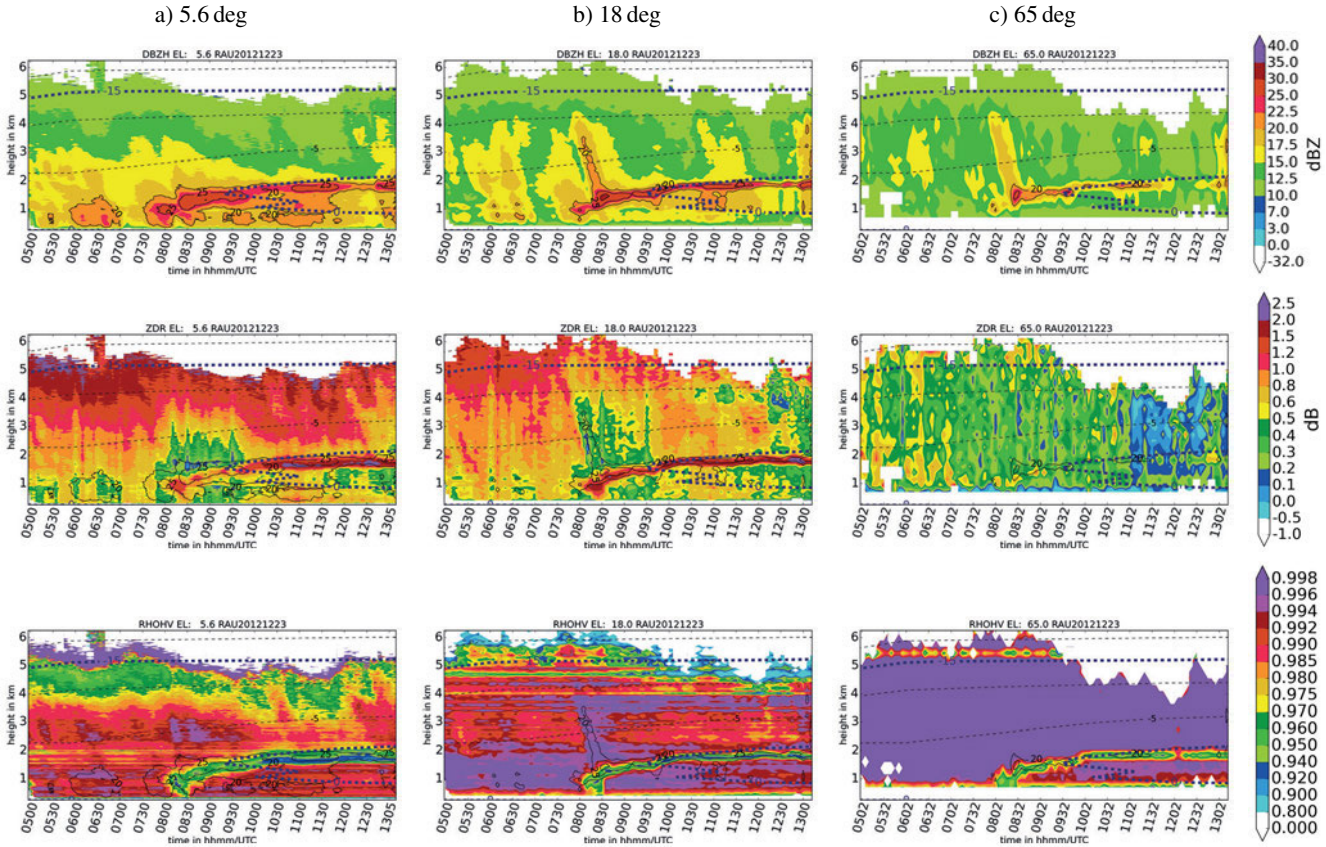

Figure 11: As in Fig. 5 but for different elevation angles. WXR RAU, 23rd December 2012, 05:00–13:00 UTC. Top-down rows show QVPs of Z, Z_{DR} and ρ_{hv}, while columns represent elevation angles of 5.6° (a), 18° (b) and 65° (c).

There are notable differences between QVPs obtained at different elevations. As expected, the differences are larger at midlevels and near cloud tops and much smaller near the surface due to linear dependence of the horizontal resolution of QVP on the height. It is obvious that the differential reflectivity loses its discriminatory value at elevation 65° as predicted in Ryzhkov et al. (2016) (their Fig. 1). Both radar reflectivity Z and cross-correlation coefficient ρ_{hv} are less sensitive to the QVP elevation and delineate the melting layer along the frontal boundary quite well. It is not surprising that the thickness of the melting layer retrieved from a lower elevation is larger than from the higher tilt QVPs which is attributed to antenna beam broadening.

Ice accumulation on a windward side of the radome may have a dramatic impact on the azimuthal patterns of Z_{DR} and other polarimetric variables at lower antenna tilts as illustrated in Fig. 12 for El = 1.8° (bottom panels). The measurements at higher elevations typically used for QVPs are much less affected by precipitation accumulation on the surface of radome which is demonstrated by the composite PPI at El = 18° (top panels in Fig. 12).

Such radome-induced artefacts, including sudden Φ_{DP} jumps around 10:00–11:00 UTC in Fig. 5, can be well captured in the QVP plots.

Analysis of the three QVPs shows that the elevation of 18° is a good compromise between horizontal resolution and information content of QVPs. Indeed, Z_{DR} is still sufficiently high at 18° and important storm features are efficiently resolved at the altitudes less than 3–4 km. At El = 18°, the horizontal resolution of QVP is about 13 km at the height of 2 km where the most informative features of the storm are located. A horizontal extension of the transition area between SN and FZRA is about 15 km as can be seen from the composite PPIs and RHIs in Fig. 7. Therefore, such a frontal transition can be easily resolved by the QVP analysis using the data at elevation 18°. In the future, we can further improve a horizontal resolution of QVP by using azimuthal averaging over limited sectors rather than full 360° circle.

3.4 Nowcasting potential of polarimetric QVPs

Since the QVP methodology captures vertical structure and evolution of the storm, it has strong potential for nowcasting of hazardous weather phenomena at the surface. As an example, a bulk of stratiform precipitation is formed initially as snow in the dendritic growth layer (DGL) and K_{DP} and Z_{DR} enhancement in DGL generally

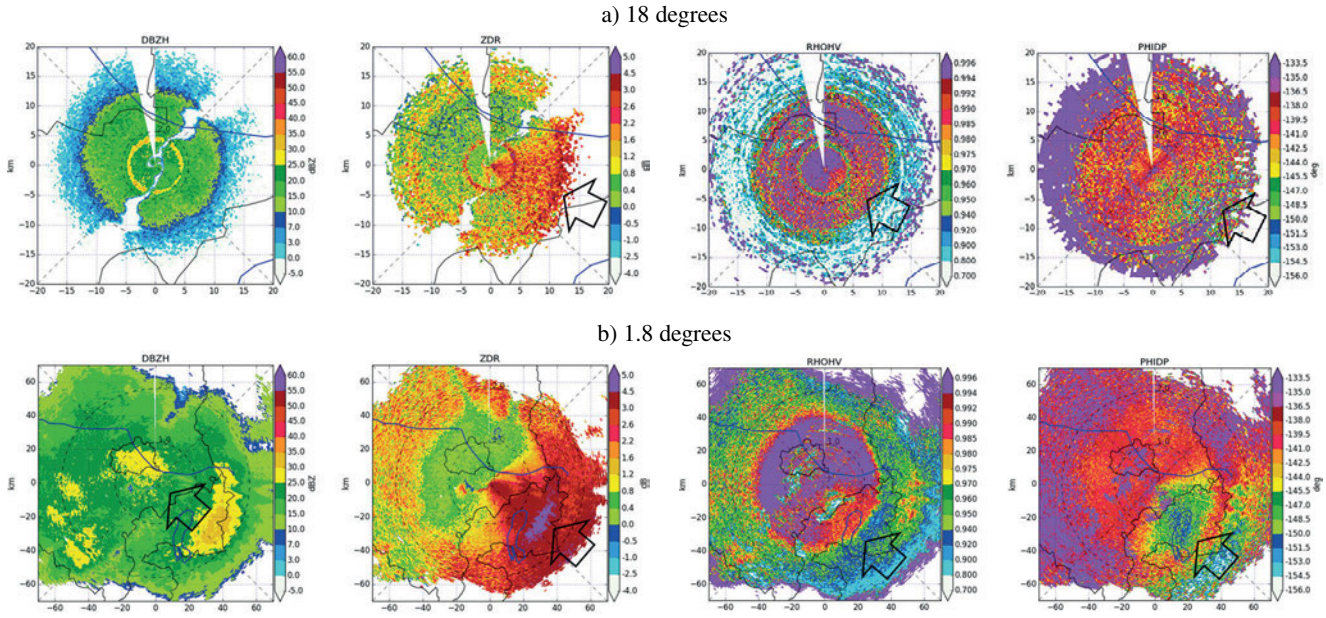

Figure 12: Composite PPI plots of Z, Z_{DR}, ρ_{hv}, and Φ_{DPDP} at elevations a) 18° and b) 1.8° from WXR RAU on 23rd Dec.2012, 11:25 UTC during freezing rain at the radar site. Location of radar in each panel is at 0,0 in meridional and zonal axis and the range is given in km (in a: +/−20 km; in b: +/−70 km). Arrows mark radome influences on polarized moments due to freezing rain accumulated at the windward side of the radome, showing a decrease of Z, enhanced Z_{DR}, and reduced ρ_{hv}/Φ_{DPDP} in the SE sector.

precedes intensification of precipitation at the ground (Kennedy and Rutledge, 2011).

On the other hand, the use of upstream QVPs offers the possibility to analyze the trend of the melting layer height and transition between different types of surface precipitation. In our case, WXR FEL (Fig. 6) shows the rapid increase in freezing level height around 23:00 UTC, i.e., about 9 hours earlier than WXR RAU at a distance of 300 km to the west. Upstream QVPs and the extrapolation of surface frontal analyses in PPIs (Fig. 7) can be well used for nowcasting of MFL accompanied by the transition from SN to PL, FZRA and later to RA for LOWW and surrounding areas (e.g., Bratislava Airport 50 km east of Vienna) and subsequent change in visibility might be forecasted as well.

A QVP product is radar-centric and we believe that its modification, a non-radar-centric Column Vertical Profile (CVP) product might be even better suited for nowcasting. Similar to QVP, the CVP implies representation of the polarimetric radar data in a height vs time format and also uses azimuthal averaging of the radar data (although in a limited azimuthal sector). As opposed to QVP, all available elevation tilts are used instead of a single one and radar data from a certain range interval are stuck vertically to produce continuous vertical profiles of radar variables. An example of a CVP of the correlation coefficient ρ_{hv} attributed to the vertical column with the base enclosed in the range interval between 30 and 40 km and azimuthal sector between 260 and 280° is presented in Fig. 13. Since such vertical column of the atmosphere is between 30 and 40 km upstream from LOWW, the corresponding CVP product can be used to predict what would happen at LOWW with 1 to 1.5 hours of lead time. The vertical resolution of the CVP product degrades with the distance from the radar which restricts lead time.

4 Conclusions

An extraordinary, strong impact winter weather event accompanied by the transition from snow to ice pellets and freezing rain at the Vienna International Airport was investigated using the Austrian C-band polarimetric weather radar data complemented with the analysis of the wind profiler data. The transformation of snow to freezing rain at the surface occurred when the warm frontal air aloft created a temperature inversion (or "warm nose") which facilitates melting of snow with resulting raindrops or ice pellets falling into cold surface layer causing icing at the surface.

A recently developed quasi-vertical profiles (QVP) methodology (Ryzhkov et al., 2016) was used for analysis of polarimetric radar data. The use of the QVP methodology allows revealing important microphysical features of the storm and their evolution which are difficult to detect using routine radar data analyses tools. These features include the dendritic growth layer and riming regions above the freezing level and the melting layer and its evolution with good accuracy and high vertical resolution.

Although the QVP methodology implies a certain degree of horizontal homogeneity of the atmosphere, it is demonstrated that the horizontal resolution of the QVPs retrieved from the data collected at antenna tilts of 15–18° is sufficient to monitor the passage of the mesoscale frontal boundaries associated with the cold

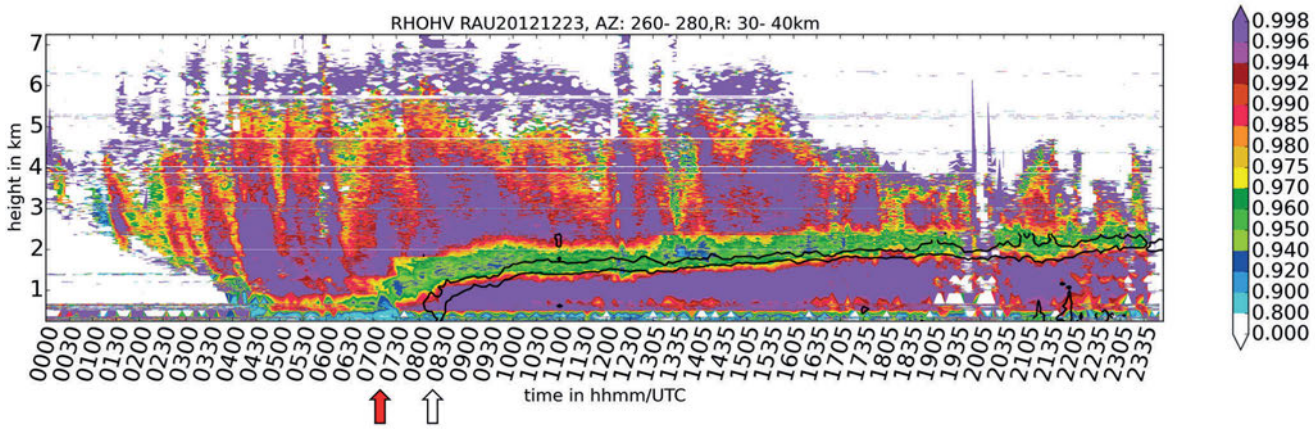

Figure 13: Example of a column vertical profile (CVP) of ρ_{hv} for the area enclosed in a range interval between 30 and 40 km in the azimuthal sector between 260 and 280° with respect to WXR RAU. The melting layer descended to the surface around 07:00 UTC in the area upstream of WXR RAU (marked by red arrow) which is approximately one hour earlier as detected by QVP at WXR RAU (marked by white arrow). The contour of ρ_{hv} = 0.94 retrieved in QVP shown in Fig. 5 is overlaid with black line.

season transitional weather events. Similar QVP analysis of the data from the radar near the Salzburg airport displays very similar features of the storm system as in the Vienna area but with warmer surface temperature which prevents icing at the surface.

Because the QVP polarimetric radar data are represented in a height vs time format which is fully compatible with the format the data from vertically pointing remote sensors such as cloud radars or wind profilers are displayed, their combined use is very efficient for understanding and monitoring microphysical processes leading to precipitation formation. This is demonstrated by the joint analysis of the polarimetric and profiler data at the Vienna airport.

The QVP methodology is particularly effective for monitoring weather in the terminal areas of airports because of its local coverage and high precision as well as its potential for nowcasting. The methodology is very easy to implement and its use along with traditional techniques for weather radar data analysis using PPIs and reconstructed RHIs looks very promising. Using upstream column vertical profile (CVP) product which is a modification of a QVP product resulted in a lead time of more than 1 hour for predicting the onset of freezing rain in our case.

Acknowledgements

Austrian weather radar network is maintained and operated by Austro Control, the national air service provider. The authors would also like to thank Peter Rafelsberger, Austro Control, for providing Austrian METAR statistics of freezing rain. We are grateful to Dirk Zinkhahn, German weather service, for providing vertical profiles of COSMO-EU numerical model data and Martin Steinheimer, Austro Control for providing analyses and forecasts of vertical profiles of ECMWF model data. Additional thanks are extended to the Austrian national meteorological service ZAMG for launching additional radio soundings in Vienna for this particular day and to the two anonymous reviewers for their careful reading and valuable comments, which improved the quality of the paper.

References

Austro Control, 2016: Aerodrome climatological summary. – LOWW/MODEL WX 2006–2015 Januar 01–March 31 and 2005–2014 October 01–December 31.

Andrić, J., M. Kumjian, D. Zirnić, J. Straka, V. Melnikov, 2013: Polarimetric signatures above the melting layer in winter storms: An observational and modeling study. – J. Appl. Meteor. Clim. **52**, 682–700.

Baumann-Stanzer, K., 2003: Qualitätsprüfung, Verifikation und Anwendung von Windprofilerdaten in Österreich. – Dissertation, University of Vienna, Austria.

Bechini, R., L. Baldini, V. Chandrasekar, 2013: Polarimetric radar observations in the ice region of precipitating clouds at C-band and X-band radar frequencies. – J. Appl. Meteor. Clim. **52**, 1147–1169.

Cortinas, J., B. Bernstein, C. Robbins, J. Strapp, 2004: An Analysis of Freezing Rain, Freezing Drizzle, and Ice Pellets across the United States and Canada: 1976–90. – Wea. Forecast. **19**, 377–390.

COSMO consortium, 2016: Consortium for Small-scale Modeling. – Aavailable online at http://www.cosmo-model.org/content/default.htm.

Diendorfer, G., R. Kaltenboeck, M. Mair, H. Pichler, 2006. Characteristics of tower lightning flashes in a winter thunderstorm and related meteorological observations. – Proceedings, 19th International Lightning Detection Conference and 1st International Lightning Meteorology Conference, Tucson, USA, 1–6.

ECMWF, 2015: CY38R1 Official IFS Documentation. – Available at https://software.ecmwf.int/wiki/display/IFS/CY38R1+Official+IFS+Documentation.

Ellis, S., and Coauthors, 2012: Towards the Detection of Aircraft Icing Conditions Using Operational Dual-polarimetric Radar. – Extended Abstracts, 7th Europ. Conference on Radar in Meteorology and Hydrology, Toulouse, France, 6 pp.

Eurocontrol, 2012: Directorate Network Management. Network Operations Report Winter 2011–2012. – Available at http://www.eurocontrol.int/publications/network-operations-winter-report-2011-2012.

Eurocontrol, 2013: Directorate Network Management. Monthly Network Operations Report. Overview December 2012. – Available at http://www.eurocontrol.int/sites/default/files/publication/performance/201212/network-operations-report-december-2012-overview.pdf.

Fabry, F., I. Zawadzki, S. Cober, G. Isaac, T. Ratvasky, F. Solheim, 2003: Detection of In-flight Icing Conditions by Radar over an Airport. – SAE Technical Paper 2003-01-2095, DOI:10.4271/2003-01-2095.

Giangrande, S., J. Krause, A. Ryzhkov, 2008: Automatic designation of the melting layer with a polarimetric prototype of the WSR-88D radar. – J. Appl. Meteor. Clim. **47**, 1354–1364.

Giangrande, S., T. Toto, A. Bansemer, M. Kumjian, S. Mishra, A. Ryzhkov, 2016: Insights into riming, aggregation, and secondary nucleation processes as revealed by aircraft, radar, and disdrometer observations for a 27 April 2011 widespread precipitation event. – J. Geophys. Res. **121**, 5846–5863.

Grazioli, J., G. Lloyd, L. Panziera, P. Connolly, J. Henneberger, A. Berne, 2015: Riming in winter alpine snowfall during CLACE 2014: polarimetric radar and in-situ observations. – Atmos. Chem. Phys. Discuss. **15**, 18065–18108.

Griffin, E., T. Schuur, A. Ryzhkov, H. Reeves, J. Picca, 2014: A Polarimetric and Microphysical Investigation of the Northeast Blizzard of 8–9 February 2013. – Wea. Forecast. **29**, 1271–1294.

Hudak, D., P. Rodrigues, G. Lee, A. Ryzhkov, F. Fabry, N. Donaldson, 2006: Winter precipitation studies with a dual polarized C-band radar. – Proceedings of the Fourth European Conference on Radar in Meteorology and Hydrology. Barcelona, Spain, 9–16.

Ikeda, K., R. Rasmussen, E. Brandes, T. McDonough, 2009: Freezing Drizzle Detection with WSR-88D Radars. – J. Appl. Meteor. Clim. **48**, 41–60

Isaac, G., and Coauthors, 2005: Nowcasting airport winter weather: AVISA tests during ARIS. – Extended Abstracts, Symp. on Nowcasting and Very Short Range Forecasting (WSN05), Toulouse, France. World Weather Research Programme, 10 pp.

Isaac, G., and Coauthors, 2014: The Canadian Airport Nowcasting System (CAN-Now). – Meteor. Appl. **21**, 30–49.

Kaltenboeck, R., 2012a: New generation of dual polarized weather radars in Austria. – Extended Abstracts, 7th Europ. Conference on Radar in Meteorology and Hydrology, Toulouse, France.

Kaltenboeck, R., 2012b: Das österreichische Wetterradarnetzwerk. – OEGMBulletin, 2012-2, 14–22. Austrian Meteor. Soc., available at http://meteorologie.at/docs/OEGM_bulletin_2012_2.pdf.

Kaltenboeck, R., A. Ryzhkov, 2013: Comparison of polarimetric signatures of hail at S and C bands for different hail sizes. – Atmos. Res. **123**, 323–336.

Kaltenboeck, R., M. Kerschbaum, K. Hennermann, S. Mayer, 2010: Applications and Visualisation of Ensemble Weather Radar Extrapolation in Austrian Aviation Weather Service Provision. – Extended Abstracts, 6th Europ. Conference on Radar in Meteorology and Hydrology, Sibiu, Rumania.

Kaltenboeck, R., M. Kraft, V. Meyer, C. Tavolato, L. Tüchler, 2015: Toward an Austrian dual-pol radar network. The Austrian TUNDRA project. – 37th Conf. on Radar Meteorology, Norman, OK, Amer. Meteor. Soc.

Keis, F., 2015: WHITE–Winter hazards in terminal environment: An automated nowcasting system for Munich Airport. – Meteorol. Z. **24**, 61–82.

Kennedy, P., S. Rutledge, 2011: S-band dual-polarization radar observations of winter storms. – J. Appl. Meteor. Clim. **50**, 844–858.

Köhler, F., U. Görsdorf, 2014: Towards 3D prediction of supercooled liquid water for aircraft icing: Modifications of the microphysics in COSMO-EU. – Meteorol. Z. **23**, 253–262.

Kumjian, M., A. Ryzhkov, H. Reeves, T. Schuur, 2013: Dual-polarization radar observations of hydrometeor refreezing in winter storms. – J. Appl. Meteor. Clim. **52**, 2549–2566.

Kumjian, M., S. Mishra, S. Giangrande, T. Toto, A. Ryzhkov, A. Bansemer, 2016: Polarimetric radar and aircraft observations of saggy bright band during MC3E. – J. Geophys. Res. Atmos. **121**, 3584–3607.

Mäkelä, A., E. Saltikoff, J. Julkunen, I. Juga, E. Gregow, S. Niemelä, 2013: Cold Season Thunderstorms in Finland and their effect on Aviation Safety. – Bull. Amer. Meteor. Soc. **94**, 847–858.

Picca, J., D. Schultz, B. Colle, S. Ganetis, D. Novak, M. Sienkiewicz, 2014: The value of dual-polarization radar in diagnosing the complex microphysical evolution of an intense snowband. – Bull. Amer. Meteor. Soc. **95**, 1825–1834.

Plummer, D., S. Goeke, R. Rauber, L. DiGirolamo, 2010: Discrimination of mixed-versus ice-phase clouds using dual-polarization radar with application to detection of aircraft icing regions. – J. Appl. Meteor. Clim. **49**, 920–935.

Rasmussen, R., J. Vivekanandan, J. Cole, B. Meyers, C. Masters, 1999: The Estimation of Snowfall Rate Using Visibility. – J. Appl. Meteor. **38**, 1542–1563.

Reeves, H., K. Elmore, A. Ryzhkov, T. Schuur, J. Krause, 2014: Sources of Uncertainty in Precipitation-Type Forecasting. – Wea. Forecast. **29**, 936–953.

Reeves, H., A. Ryzhkov, J. Krause, 2016: Discrimination between winter precipitation types based on spectral-bin microphysical modeling. – J. Appl. Meteor. Clim. **55**, 1747–1761.

Ryzhkov, A., H. Reeves, T. Schuur, M. Kumjian, D. Zrnić, 2011: Investigations of polarimetric radar signatures in winter storms and their relation to aircraft icing and freezing rain. – Extended Abstracts, 35th Conf. on Radar Meteorology, Pittsburgh, PA, Amer. Meteor. Soc., P13.197.

Ryzhkov, A., H. Reeves, J. Krause, H. Burcham, 2014: Discrimination between winter precipitation types based on explicit microphysical modeling of melting and refreezing in the polarimetric hydrometeor classification algorithm. – Extended abstracts. 8th European Conference on Radar in Meteorology and Hydrology, Garmisch-Partenkirchen, Germany, MIC.P07.

Ryzhkov, A., P. Zhang, H. Reeves, M. Kumjian, T. Tschallener, S. Troemel, C. Simmer, 2016: Quasi-vertical profiles–a new way to look at polarimetric radar data. – J. Atmos. Oceanic Technol. **33**, 551–562.

Schulz, J., U. Schättler, 2014: Kurze Beschreibung des Lokal-Modells Europa COSMO-EU (LME) und seiner Datenbanken auf dem Datenserver des DWD. – Available at http://www.dwd.de/SharedDocs/downloads/DE/modelldokumentationen/nwv/cosmo_eu/cosmo_eu_dbbeschr_201406.pdf;jsessionid=0B509D2AF05F0B77D5FC1B29ED22CB4C.live21063?__blob=publicationFile&v=3.

Schuur, T., H. Park, A. Ryzhkov, H. Reeves, 2012: Classification of precipitation types during transitional winter weather using the RUC model and polarimetric radar retrievals. – J. Appl. Meteor. Clim. **51**, 763–779.

Schuur, T., A. Ryzhkov. H. Reeves, J. Krause, K. Elmore, K. Ortega, 2014: Recent modifications to a new surface-based polarimetric Hydrometeor Classification Algo-

rithm for the WSR-88D network. – Extended abstracts. 8th European Conference on Radar in Meteorology and Hydrology, Garmisch-Partenkirchen, Germany, 7 pp.

Serke, D., J. Hubbert, S. Ellis, A. Reehorst, P. Kennedy, D. Albo, A. Weekley, M. Politovich, 2011: The winter 2010 FRONT/NIRSS in-flight icing detection field campaign. – 35th Conference on Radar Meteorology, Pittsburgh, PA, Amer. Meteor. Soc.

Teshiba, M., P. Chilson, A. Ryzhkov, T. Schuur, R. Palmer, 2009: A combined wind profiler and polarimetric weather radar method for the investigation of precipitation and vertical velocities. – J. Atmos. Oceanic Technol. **26**, 1940–1955.

Thompson, E., S. Rutledge, B. Dolan, V. Chandrasekhar, B. Cheong, 2014: A dual-polarization radar hydrometeor classification algorithm for winter precipitation. – J. Atmos. Oceanic Technol. **31**, 1457–1481.

Troemel, S., A. Ryzhkov, P. Zhang, C. Simmer, 2014: Investigations of backscatter differential phase in the melting layer. – J. Appl. Meteor. Clim. **53**, 2344–2359.

Vogel, J., F. Fabry, I. Zawadzki, 2015: Attempts to observe polarimetric signatures of riming in stratiform precipitation. – 37th Conf. on Radar Meteorology, Norman, OK, Amer. Meteor. Soc. 6B.6, available at https://ams.confex.com/ams/37RADAR/webprogram/Paper275246.html.

Williams, E. and Coauthors, 2015: Measurements of differential reflectivity in snowstorms and warm season stratiform systems. – J. Appl. Meteor. Clim. **54**, 573–595.

WMO, 2007: World Meteorological Organisation–Aviation Hazards. – Education and Training Programme, ETR-20, WMO-TD-No.1390, available at http://www.caem.wmo.int/moodle/file.php?file=/1/AVIATION_HAZARDS.pdf.

ZAMG, 2015: Aktuelle Wetterkarte und Kartenarchiv. – Available at https://www.zamg.ac.at/cms/de/wetter/wetterkarte?tag=23&monat=12&jahr=2012&utc=12.

Zawadzki, I., W. Szyrmer, C. Bell, F. Fabry, 2005: Modeling of the Melting Layer. Part III: The Density Effect. – J. Atmos. Sci. **62**, 3705–3723.

Zerr, R., 1997: Freezing rain: an observational and theoretical study. – J. Appl. Meteor. **36**, 1647–1661.